Check for updates

A simple synthesis of Ga_2O_3 and GaN nanocrystals†

Erwei Huang,[a] Juxia Li,[a] Guangjun Wu,[a] Weili Dai, [iD][a] Naijia Guan[ab] and Landong Li [iD] *[ab]

The synthesis of gallium oxide and nitride nanocrystals is challenging. Herein, a forced hydrolysis route is developed to synthesize α-GaOOH and the morphology control of nanocrystals is realized by adjusting the ratios of ionic strength in the synthesis system. The as-prepared α-GaOOH nanorods can be transformed into α-Ga_2O_3 nanorods upon calcination and can be further transformed into GaN nanocrystal assemblies through nitridation at elevated temperatures, which provides a top-down strategy to gallium oxide and nitride nanocrystals. The synthesis results are investigated by means of X-ray diffraction (XRD), Raman spectroscopy, scanning electron microscopy (SEM) and transmission electron microscopy (TEM). The optical properties, *i.e.* ultra-violet visible absorption (UV-vis) and photoluminescence, of as-obtained α-Ga_2O_3 nanocrystals with different morphologies are examined and the morphology–property relationship is discussed.

Introduction

Gallium oxide (Ga_2O_3) and nitride (GaN) are wide band-gap semiconductors with energy gaps of ∼4.6 and ∼3.4 eV, respectively.[1,2] Both have attracted considerable interest for potential applications in spintronic, electronic and optoelectronic devices due to their intrinsic properties.[3–7] The morphologies of these materials show significant impacts on their properties, and, therefore, they have received extensive attention in past decades.[8–10] Various morphologies of GaN nanocrystals, *e.g.* nanowires, nanorods, nanotubes, nanobelts and nanohollows, have been successfully constructed and applied as electronic or optoelectronic devices.[11–16] For example, Fan *et al.* prepared GaN nanorods through a confined reaction by using Ga_2O vapour and NH_3 gas in the presence of carbon nanotubes as templates.[11] Yang *et al.* developed a chemical vapour deposition route to synthesize single GaN nanowire on sapphire substrate and further explored its promising applications in lasers.[14] Subsequently, they reported the epitaxial growth of single-crystal GaN nanotubes by adopting hexagonal ZnO nanowires as templates also through chemical vapour deposition.[17] Chou *et al.* prepared GaN nanobelts through Au-assisted nucleation and non-Au-assisted anisotropy vapor–solid growth on $LiAlO_2$ substrate.[18] In addition, other strategies, *e.g.* metalorganic vapor phase epitaxy[19] and rapid thermal ammonolysis of complex gallium fluoride,[20,21] have been reported for the synthesis of GaN and doped GaN nanostructures.

According to these reports, it can be seen that the synthesis of GaN nanostructures always involves expensive and/or poisonous reagents, templates or substrates, and complicated processes.[18–23] It is known that the nitridation of Ga_2O_3 represents a most simple strategy to free-standing GaN material. Theoretically, the morphology of parent Ga_2O_3 material can be preserved under controlled nitridation conditions, which provides a top-down morphology control strategy to GaN. It has been already reported that Ga_2O_3 nanorods can be synthesized *via* a thermal decomposition method using GaOOH nanorods.[24] Moreover, GaN nanoparticles can be produced from Ga_2O_3 nanoparticles under a flow of ammonia gas at elevated temperatures.[25]

Inspired by these achievements, we herein report a so-called forced hydrolysis route to GaOOH nanorods, which can be transformed to Ga_2O_3 nanorods through calcination and be further transformed to GaN nanocrystal assembles through nitridation. During the forced hydrolysis process, the hydroxyls are produced from urea decomposition[26] and morphology control of GaOOH is realized by adjusting the ratio of ionic strength in the synthesis system.

Experimental

Synthesis of Ga_2O_3 and GaN samples

All the chemical reagents were of analytical reagent grade and directly used without further purification. GaOOH was prepared *via* a forced hydrolysis route starting from solution containing $Ga(NO_3)_3$ and $NaNO_3$ with different ionic strength ratios (see below for details).

Ionic strength (I) is calculated by the formula of $I \underset{=}{\mathrm{def}} \frac{1}{2} \sum_B m_B z_B{}^2$, where m_B is the molality of an ion B in the solution and Z_B is its charge number (positive for cations and

[a]School of Materials Science and Engineering, National Institute for Advanced Materials, Nankai University, Tianjin, 300350, P. R. China

[b]Key Laboratory of Advanced Energy Materials Chemistry (Ministry of Education), Collaborative Innovation Center of Chemical Science and Engineering, Tianjin, 300071, P. R. China. E-mail: lild@nankai.edu.cn

negative for anions). The ratio of ionic strength (R) is defined as $R = \dfrac{I_1}{I_2}$, where I_1 represents the ionic strength of $Ga(NO_3)_3$ in the solution and I_2 represents the ionic strength of $NaNO_3$ in the solution.

In a typical synthesis, an appropriate amount of $Ga(NO_3)_3 \cdot nH_2O$ and urea were dissolved into a small amount of deionized water (the molar ratio of $Ga(NO_3)_3 \cdot nH_2O$ and urea being kept at 1 : 6) and heated to 90 °C. More deionized water was then added to reach a final molarity of urea is 0.18 mol L^{-1} (Ga^{3+} of 0.03 mol L^{-1}) and the temperature was kept at 90 °C for 9 h to initiate forced hydrolysis. The solid product was centrifuged, thoroughly washed, dried and defined as GaOOH ($R = \infty$). The as-obtained GaOOH was calcined in the vacuum at 450 °C to derive Ga_2O_3, which was further nitridized in NH_3 flow (100 mL min^{-1}) at 950 °C for 6 h to derive GaN. With the addition of $NaNO_3$ into $Ga(NO_3)_3 \cdot nH_2O$ solution at different ionic strength ratios, GaOOH products ($R = 3, 2, 1, 0.5, 0.3$ or 0.2), were obtained, which could also be transformed to Ga_2O_3 and GaN samples ($R = 3, 2, 1, 0.5, 0.3$ or 0.2) via identical procedures.

For reference, commercial Ga_2O_3 (defined as Raw) was nitridized at 950 °C for 6 h to derive GaN.

Characterization of Ga_2O_3 and GaN samples

The X-ray diffraction (XRD) patterns of samples were acquired on a Rigaku Smart Lab 3 kW powder diffractometer with Cu Kα radiation ($\lambda = 0.1542$ nm) at a scanning rate of 6° min^{-1}.

The specific surface areas of samples were determined through N_2 physisorption at 77 K on a Quantachrome iQ-MP gas adsorption analyzer.

Scanning electron microscopy (SEM) images of Ga_2O_3 and GaN samples were obtained on a JSM-7500F electron microscope.

Transmission electron microscopy (TEM) and high-resolution transmission electron microscopy (HRTEM) images of Ga_2O_3 and GaN samples were obtained on a FEI Tecnai G^2 F20 electron microscope at 200 kV. Alcohol suspensions containing the Ga_2O_3 or GaN were dropped onto a carbon-coated copper grid, followed by evaporation at ambient temperature.

The Raman spectra of Ga_2O_3 and GaN were recorded on a Renishaw InVia Raman spectrometer with the green line of an Ar-ion laser (514.53 nm) in micro-Raman configuration.

Diffuse reflectance ultra-violet visible absorption (UV-vis) spectra of Ga_2O_3 and GaN samples were performed on a Varian Cary 300 UV/vis spectrophotometer.

Photoluminescence spectra of Ga_2O_3 and GaN samples were acquired on a Spex FL201 fluorescence spectrophotometer. Self-supporting wafers of samples (ca. 100 mg) were excited by 270 nm laser and the spectra were recorded in vacuum at ambient temperature.

Results and discussion

The XRD patterns of GaOOH, Ga_2O_3 and GaN samples prepared at $R = 1$ are shown in Fig. 1. It can be seen that pure orthorhombic phase α-GaOOH is obtained from forced hydrolysis (JCPDS no. 06-0180; $a = 4.58$ Å, $b = 9.80$ Å, $c = 2.97$ Å). GaOOH can be

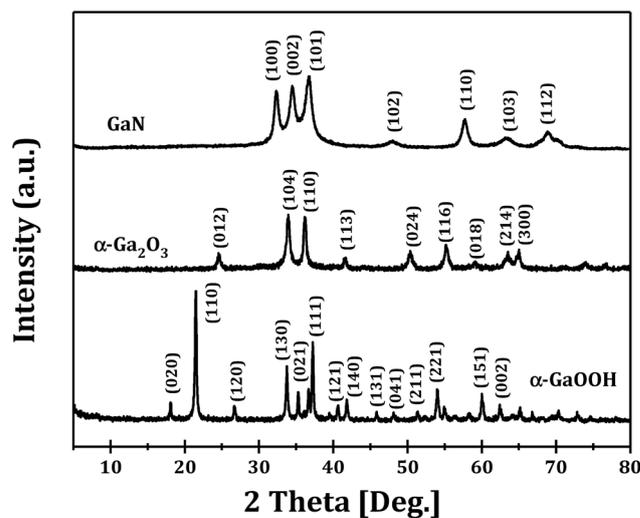Fig. 1 XRD patterns of GaOOH, Ga_2O_3 and GaN prepared at $R = 1$.

transformed to pure hexagonal phase α-Ga_2O_3 (JCPDS no. 06-0503; $a = b = 4.98$ Å, $c = 13.43$ Å) upon calcination at 450 °C and Ga_2O_3 can be transformed to pure hexagonal phase GaN (JCPDS no. 50-0792; $a = b = 3.19$ Å, $c = 5.19$ Å) upon nitridation at 950 °C. These results clearly demonstrate the feasibility of Ga_2O_3 and GaN synthesis through a so-called top-down strategy.

Fig. 2 shows the XRD patterns of Ga_2O_3 samples synthesized via forced hydrolysis at different R values and followed by calcination. All the samples exhibit similar diffraction peaks of α-Ga_2O_3 (JCPDS no. 06-0503), a monoclinic system and $C2/m$ space group with $a = b = 4.98$ Å and $c = 13.43$ Å as its cell parameters.[27] No diffraction peaks corresponding to impurity phases can be observed in all cases. We notice that, however, the intensities of diffraction peaks of Ga_2O_3 samples synthesized at different R values are different, indicating that different morphologies and/or crystallinities were obtained for these Ga_2O_3 samples. With increasing R value from 0.2 to 1, the
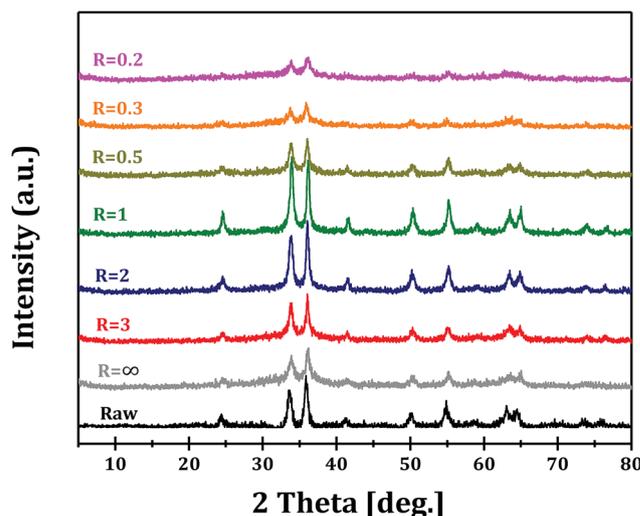

Fig. 2 XRD patterns of Ga_2O_3 synthesized at different R values and Raw Ga_2O_3.

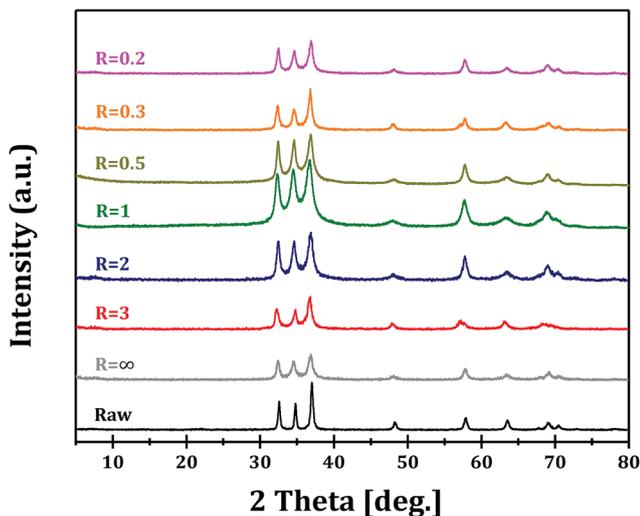**Fig. 3** XRD patterns of GaN from the nitridation of Ga_2O_3 synthesized at different R values and Raw Ga_2O_3.

Fig. 4 SEM images of Ga_2O_3 synthesized at different R values: $R = \infty$ (a); $R = 3$ (b); $R = 2$ (c); $R = 1$ (d); $R = 0.5$ (e); $R = 0.3$ (f); $R = 0.2$ (g) and Raw Ga_2O_3 (h).

relative crystallinity increases distinctly, while the relative crystallinity decreases with further increase in R value. That is, Ga_2O_3 with highest crystallinity can be obtained with optimized ionic strength ratio of 1 during forced hydrolysis.

Raman spectroscopy is further employed to determine the structure of as-prepared Ga_2O_3 samples. As shown in Fig. S1,† Raman bands at 410, 560 and 700–710 cm^{-1} are observed in the 300–1000 cm^{-1} region, corresponding to the E_g, A_{1g} and E_g modes of α-Ga_2O_3, respectively.[1,28] The Raman bands broadening and the noticeable shifts of bands at 700–710 cm^{-1} are due to the presence of surface defects on the samples.

The XRD patterns of GaN samples from the nitridation of different Ga_2O_3 samples are shown in Fig. 3. Pure GaN phase of wurtzite structure and $P6_3mc$ space group with $a = b = 3.189$ Å and $c = 5.185$ Å as its cell parameters is obtained in all cases.[27] We also notice the different intensities of diffraction peaks, similar to the trend observed for Ga_2O_3 samples. It can be proposed that the morphologies and crystallinities of Ga_2O_3 samples are preserved, at least partially preserved, through nitridation at elevated temperature of 950 °C. Raman spectra of GaN samples are presented in Fig. S2† and a series of Raman bands can be observed in the 300–1000 cm^{-1} region. The band at 420 cm^{-1} is related to the N-rich structure of GaN,[29] while the shifts of other Raman bands, e.g. at 515, 595 and 695 cm^{-1}, compared with standard hexagonal GaN, should be related to the formation of abundant defects on the surface.[20]

The SEM images of Ga_2O_3 samples synthesized by forced hydrolysis at different R values are shown in Fig. 4. It is very clear that different morphologies are obtained at different ratios of ionic strength during forced hydrolysis, i.e. R values. At $R = \infty$, Ga_2O_3 crystals appear as spindle-like nanorods with two narrow sides and a wide center (Fig. 4a). At $R = 3$ and 2, Ga_2O_3 crystals appear as nanorods with the same broad sides and center (Fig. 4b and c). With decreasing R value to 1, Ga_2O_3 crystals transform to dumbbell-shaped nanorods with two wide sides and narrow center (Fig. 4d). Further decrease in the ratio
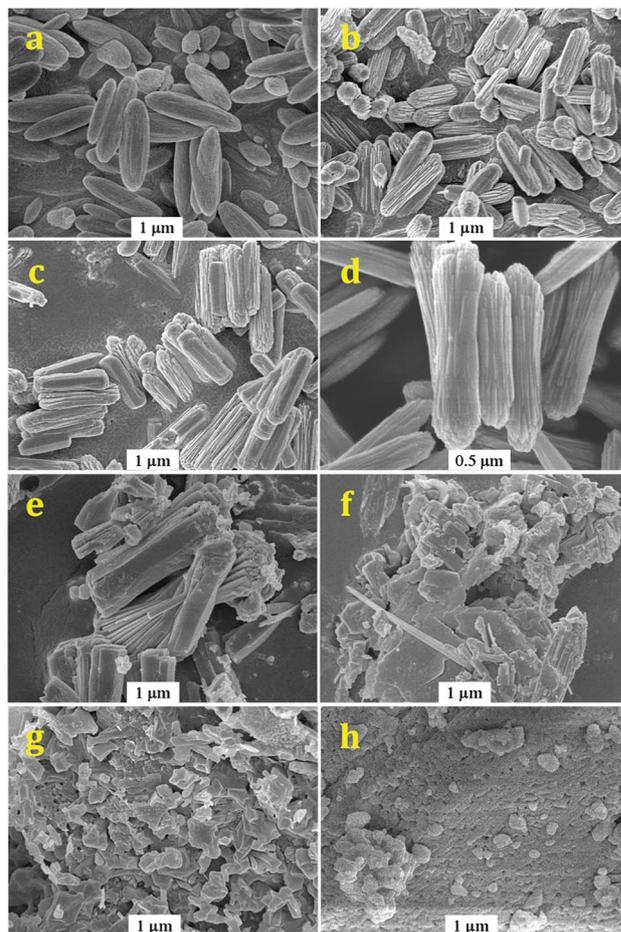
of ionic strength during forced hydrolysis ($R = 0.5$ and 0.3) results in the exfoliation of nanorods to nanoplates and strips and fragments (Fig. 4e and f). At $R = 0.2$, the Ga_2O_3 crystals are totally broken up to fragments. According to the SEM images of Ga_2O_3 samples synthesized at different R values, we can infer that the crystallinities of Ga_2O_3 samples vary with R values. The highest crystallinity of Ga_2O_3 sample is obtained at the R value of 1, in accordance with the results from XRD patterns (Fig. 2). The surface areas of Ga_2O_3 samples synthesized at different R values are measured to be in the range of 30–50 $m^2\ g^{-1}$, distinctly higher than commercial Ga_2O_3 (15 $m^2\ g^{-1}$).

Fig. 5 shows the SEM images of GaN samples obtained from the nitridation of Ga_2O_3 samples. It is seen that the overall shape of GaN sample follows its Ga_2O_3 precursor. However, after careful observation, we find that some tiny nanoparticles do exist on the external surface of GaN crystals. These observations indicate that nitridation starts from a local point of Ga_2O_3 crystal. The surface areas of as-obtained GaN samples are measured to be 40–60 $m^2\ g^{-1}$, even higher than parent Ga_2O_3 (30–50 $m^2\ g^{-1}$) due to the formation of tiny nanoparticles on the surface. To confirm the phase purity of as-obtained GaN samples, the energy-dispersive X-ray mapping analysis was
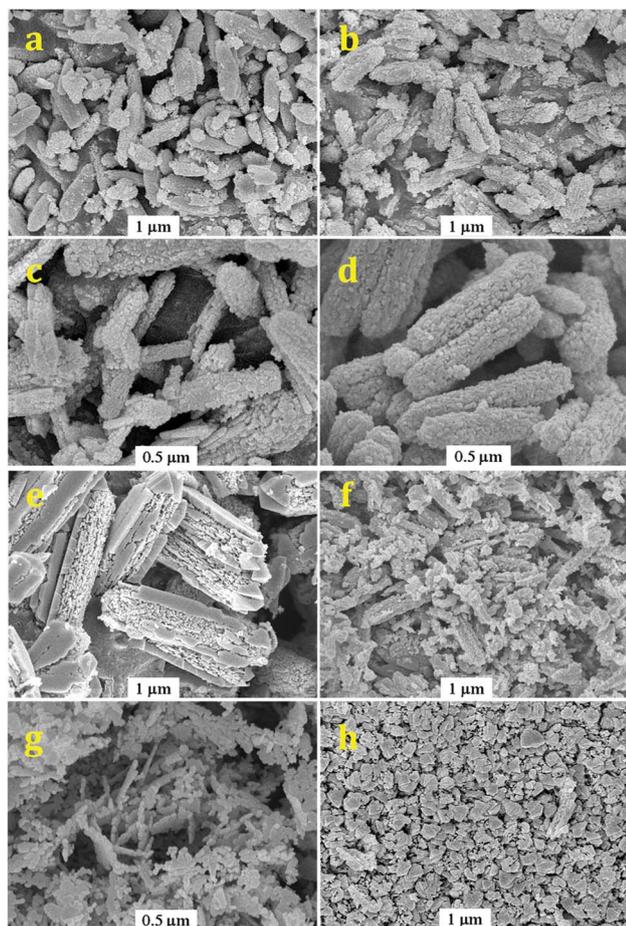
Fig. 5 SEM images of GaN from the nitridation of Ga$_2$O$_3$ synthesized at different R values: $R = \infty$ (a); $R = 3$ (b); $R = 2$ (c); $R = 1$ (d); $R = 0.5$ (e); $R = 0.3$ (f); $R = 0.2$ (g) and Raw Ga$_2$O$_3$ (h).

performed on representative GaN sample ($R = 1$). As shown in Fig. S3,† the homogeneous distribution of Ga and N species in selected GaN crystal grain is clearly observed (Ga/N = 0.86; Ga/N < 1 due to the presence of N-containing impurities), ruling out the formation of metallic Ga islands from nitridation at high temperature of 950 °C.

For a more clear view of the morphology changes during nitridation, TEM images of Ga$_2$O$_3$ and GaN samples synthesized at $R = 1$ are shown in Fig. 6. A typical Ga$_2$O$_3$ crystal assembly appears as a nanorod with length of 2 μm and diameter of 0.4 μm (Fig. 6a). In the HRTEM images (Fig. 6b and c), clear lattice fringes with interplanar spacing of 0.249 nm are observed, corresponding to the (110) planes of Ga$_2$O$_3$ crystal. After nitridation, the overall shape of Ga$_2$O$_3$ is well preserved (Fig. 6d), in accordance with SEM observations. It is also found that the GaN crystal assembly is composed of tiny nanoparticles with sizes of a few to a dozen nanometers. Accordingly, some nanoscale mesopores can be observed in GaN crystal assembly. HRTEM images (Fig. 6e and f) reveal the lattice fringes with interplanar spacing of 0.276 nm, corresponding to the (100) planes of GaN crystal.

On the basis of SEM (Fig. 4) and TEM observations (Fig. 6), we demonstrate that Ga$_2$O$_3$ samples with different morphologies

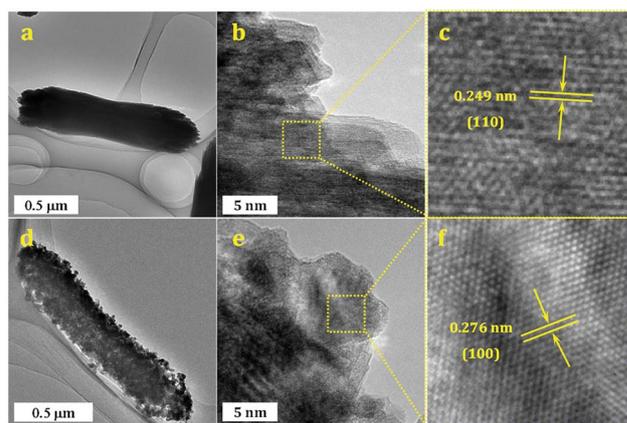Fig. 6 TEM images (a, d), HRTEM images (b, e) and enlarged view of HRTEM images (c, f) of Ga$_2$O$_3$ and GaN samples synthesized at $R = 1$.

can be prepared via controlling the ratio of ironic strength during forced hydrolysis. With decreasing R value, the morphology of Ga$_2$O$_3$ crystals gradually transforms from spindle-like to dumbbell-shaped nanorods and then to exfoliated fragments, which gives us a hint on the formation process of Ga$_2$O$_3$ sample.

A schematic diagram of morphology-controlled synthesis of Ga$_2$O$_3$ via forced hydrolysis route is summarized in Fig. 7. In the first step, different ratios of Ga(NO$_3$)$_3$·nH$_2$O, NaNO$_3$ and urea are mixed in deionized water and heated at 90 °C to form unstable Ga(OH)$_3$ transition state. Then, the unstable Ga(OH)$_3$ transition state crystallizes to different morphologies of α-GaOOH at 90 °C with the presence of different concentrations of sodium ions as structure-directing and mineralizing agents. In the final step, GaOOH is transformed to α-Ga$_2$O$_3$ through calcination in vacuum, with its morphology well preserved. Besides, the as-obtained α-Ga$_2$O$_3$ can be transformed to GaN with overall morphology well preserved (Fig. 6).

The optical properties of as-obtained α-Ga$_2$O$_3$ samples with different morphologies are examined to explore the possible morphology-dependent effects. The UV-vis spectra of α-Ga$_2$O$_3$ synthesized at different R values are shown in Fig. 8. Commercial α-Ga$_2$O$_3$ sample (Raw) shows significant absorption in the ultraviolet region with edge up to ~290 nm, corresponding to the
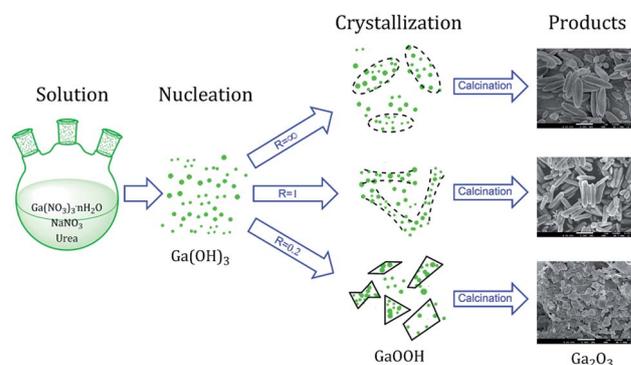

Fig. 7 Schematic diagram of morphology-controlled synthesis of Ga$_2$O$_3$ via forced hydrolysis route.

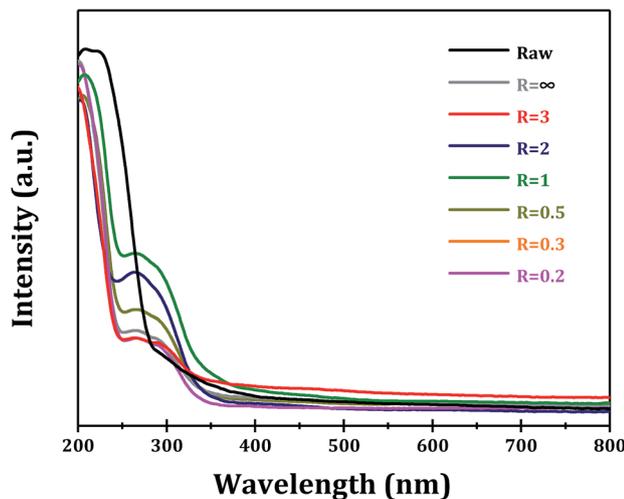Fig. 8 UV-vis spectra of Ga_2O_3 synthesized at different R values.

Fig. 9 Photoluminescence spectra of Ga_2O_3 synthesized at different R values.

band gap of ~4.3 eV. While for α-Ga_2O_3 samples prepared *via* forced hydrolysis, two absorption peaks can be distinguished, *i.e.* intrinsic absorption with edge up to ~260 nm (4.8 eV) and sub-band absorption with edge up to ~360 nm (3.5 eV). The sub-band absorption should be related with the existence of abundant defect sites in α-Ga_2O_3, *e.g.* oxygen vacancies as proposed in other oxide semiconductors.[30,31] It is seen that the highest absorption with edge up to ~360 nm is obtained with α-Ga_2O_3 sample at $R = 1$, indicating its highest defect site concentration.

For GaN samples from the nitridation of α-Ga_2O_3 samples, significant absorption in the ultraviolet and visible region is observed (Fig. S4†). The band-edge energy cannot be distinguished due to the overlap by sub-band absorption as well as the serious light scattering effects caused by the formation of mesoporous structure (Fig. 5 and 6).

The photoluminescence properties of α-Ga_2O_3 samples synthesized at different R values are examined. It is known that the photoluminescence emissions are originated from the radiative recombination of photo-generated electrons and holes on semiconductors. Two major photo-physical processes, *i.e.* direct band–band transition and indirect transition from trapping states, can give rise to photoluminescence signals. Under 270 nm ultraviolet light excitation, a broad photoluminescence signal from 350 to 700 nm (centered at 500 nm) is observed for commercial α-Ga_2O_3 sample (Fig. 9). While for α-Ga_2O_3 samples prepared *via* forced hydrolysis followed by calcination, two significant photoluminescence signals at 460 (blue photoluminescence) and 600 nm (orange photoluminescence) are observed. The blue photoluminescence signal should be originated from the recombination of photogenerated electrons on donors and holes on acceptors while the orange photoluminescence from the recombination on deep trapping states.[32,33] Undoubtedly, all these two photoluminescence signals are associated with the defect sites in as-prepared α-Ga_2O_3 samples, which distinguish them from commercial sample. In this context, the intensity of photoluminescence signals is determined by both the defect sites and the crystallinity of the sample.
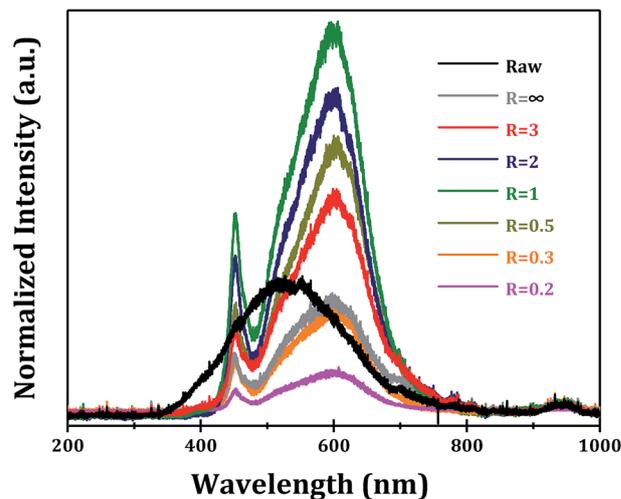
We find that the sequence of photoluminescence intensity (Fig. 9) correlates well with the optical absorption (Fig. 8), both of which indicate the morphology-dependent optical properties of α-Ga_2O_3 samples. At $R = 1$, the highest photoluminescence intensity is obtained, several times higher than commercial α-Ga_2O_3 sample.

We also investigate the optical properties of GaN samples prepared from the nitridation of α-Ga_2O_3 samples and the results are shown in Fig. S5.† Significant photoluminescence signals at 380 and 450 nm are observed for all samples in the 350–480 nm region, and the highest photoluminescence intensity is obtained with GaN ($R = 1$). Besides, we cannot draw other convincing conclusions on the morphology-dependent effects due to the serious light scattering effects caused by the formation of mesoporous structure. Further researches on these issues are still in progress.

Conclusions

In summary, we have successfully developed a forced hydrolysis route to α-GaOOH starting from inorganic gallium salt and urea as raw materials, and we have realized the morphology control by adjusting the ratios of ionic strength in the synthesis system, *i.e.* Ga^{3+}/Na^+. The as-prepared α-GaOOH nanorods can be transformed to α-Ga_2O_3 nanorods upon simple calcination with the morphology well preserved, and be further transformed to GaN nanocrystal assembles through nitridation. This process provides a top-down strategy to Ga_2O_3 and GaN nanocrystals. Typically, the morphology of as-obtained α-Ga_2O_3 crystals gradually transform from spindle-like to dumbbell-shaped nanorods and then to exfoliated fragments with decreasing ratios of ionic strength in the synthesis system. While for the GaN samples prepared from nitridation at elevated temperature, the overall shape of α-Ga_2O_3 precursor can be preserved and nanoscale mesopores originated from nanoparticles assembling are clearly observed.

The UV-vis absorption and photoluminescence properties of Ga_2O_3 crystals with different morphologies are examined, and the

results clearly demonstrate the morphology-dependent effects. The methodology presented here may be extended to the synthesis and applications of other oxide and nitride semiconductors.

Conflicts of interest

There are no conflicts to declare.

Acknowledgements

Notes and references

1 X. Wang, Q. Xu, M. Li, S. Shen, X. Wang, Y. Wang, Z. Feng, J. Shi, H. Han and C. Li, *Angew. Chem., Int. Ed.*, 2012, **51**, 13089–13092.

2 K. Maeda, T. Takata, M. Hara, N. Saito, Y. Inoue, H. Kobayashi and K. Domen, *J. Am. Chem. Soc.*, 2005, **127**, 8286–8287.

3 T. Ohno, L. Bai, T. Hisatomi, K. Maeda and K. Domen, *J. Am. Chem. Soc.*, 2012, **134**, 8254–8259.

4 P. Parkinson, C. Dodson, J. J. Joyce, K. A. Bertness, N. A. Sanford, L. M. Herz and M. B. Johnston, *Nano Lett.*, 2012, **12**, 4600–4604.

5 T. Hashimoto, F. Wu, J. S. Speck and S. Nakamura, *Nat. Mater.*, 2007, **6**, 568–571.

6 J. Hejtmánek, K. Knížek, M. Maryško, Z. Jirák, D. Sedmidubský, Z. Sofer, V. Peřina, H. Hardtdegen and C. Buchal, *J. Appl. Phys.*, 2008, **103**, 07D107.

7 Z. Sofer, D. Sedmidubský, J. Stejskal, J. Hejtmánek, M. Maryško, K. Jurek, M. Václavů, V. Havránek and A. Macková, *J. Cryst. Growth*, 2008, **310**, 5025–5031.

8 X. F. Wang, J. H. Tong, X. Chen, B. J. Zhao, Z. W. Ren, D. W. Li, X. J. Zhuo, J. Zhang, H. X. Yi, C. Liu, F. Fang and S. T. Li, *Chem. Commun.*, 2014, **50**, 682–684.

9 C. T. Huang, J. H. Song, W. F. Lee, Y. Ding, Z. Y. Gao, Y. Hao, L. J. Chen and Z. L. Wang, *J. Am. Chem. Soc.*, 2010, **132**, 4766–4771.

10 R. Zou, Z. Zhang, Q. Liu, J. Hu, L. Sang, M. Liao and W. Zhang, *Small*, 2014, **10**, 1848–1856.

11 W. Han, S. Fan, Q. Li and Y. Hu, *Science*, 1997, **277**, 1287–1289.

12 X. Sun and Y. Li, *Angew. Chem., Int. Ed.*, 2004, **43**, 3827–3831.

13 J. Wallys, J. Teubert, F. Furtmayr, D. M. Hofmann and M. Eickhoff, *Nano Lett.*, 2012, **12**, 6180–6186.

14 J. C. Johnson, H. J. Choi, K. P. Knutsen, R. D. Schaller, P. D. Yang and R. J. Saykally, *Nat. Mater.*, 2002, **1**, 106–110.

15 Y. J. Hwang, C. H. Wu, C. Hahn, H. E. Jeong and P. D. Yang, *Nano Lett.*, 2012, **12**, 1678–1682.

16 P. Huang, H. Zong, J. J. Shi, M. Zhang, X. H. Jiang, H. X. Zhong, Y. M. Ding, Y. P. He, J. Lu and X. D. Hu, *ACS Nano*, 2015, **9**, 9276–9283.

17 J. Goldberger, R. R. He, Y. F. Zhang, S. W. Lee, H. Q. Yan, H. J. Choi and P. D. Yang, *Nature*, 2003, **422**, 599–602.

18 C. L. Chen, M. M. C. Chou, T. Yan, H. C. Huang, C. Y. J. Lu and C. H. Chen, *Chem. Commun.*, 2014, **50**, 5695–5698.

19 Z. Sofer, D. Sedmidubský, Š. Huber, J. Hejtmánek, A. Macková and R. Fiala, *Int. J. Nanotechnol.*, 2012, **9**, 809–824.

20 Z. Sofer, D. Sedmidubský, Š. Huber, P. Šimek, F. Šaněk, O. Jankovský, E. Gregorová, R. Fiala, S. Matějková and M. Mikulics, *J. Nanopart. Res.*, 2013, **15**, 1411.

21 P. Šimek, D. Sedmidubský, Š. Huber, K. Klímová, M. Maryško, M. Mikulics and Z. Sofer, *Mater. Chem. Phys.*, 2015, **164**, 108–114.

22 X. Chen, J. Xu, R. M. Wang and D. Yu, *Adv. Mater.*, 2003, **15**, 419–421.

23 Y. Xie, Y. Qian, W. Wang, S. Zhang and Y. Zhang, *Science*, 1996, **272**, 1926–1927.

24 X. Liu, G. Qiu, Y. Zhao, N. Zhang and R. Yi, *J. Alloys Compd.*, 2007, **439**, 275–278.

25 T. Ogi, Y. Kaihatsu, F. Iskandar, E. Tanabe and K. Okuyama, *Adv. Powder Technol.*, 2009, **20**, 29–34.

26 W. H. R. Shaw and J. J. Bordeaux, *J. Am. Chem. Soc.*, 1955, **77**, 4729–4733.

27 M. Muruganandham, R. Amutha, M. S. M. A. Wahed, B. Ahmmad, Y. Kuroda, R. P. S. Suri, J. J. Wu and M. E. T. Sillanpää, *J. Phys. Chem. C*, 2012, **116**, 44–53.

28 D. Machon, P. F. McMillan, B. Xu and J. Dong, *Phys. Rev. B*, 2006, **73**, 094125.

29 J. Q. Ning, S. J. Xu, D. P. Yu, Y. Y. Shan and S. T. Le, *Appl. Phys. Lett.*, 2007, **91**, 103117.

30 J. Yan, T. Wang, G. Wu, W. Dai, N. Guan, L. Li and J. Gong, *Adv. Mater.*, 2015, **27**, 1580–1586.

31 L. Li, J. Yan, T. Wang, Z. J. Zhao, J. Zhang, J. Gong and N. Guan, *Nat. Commun.*, 2015, **6**, 5881.

32 T. Harwig and F. Kellendonk, *J. Solid State Chem.*, 1978, **24**, 255–263.

33 L. Binet and D. Gourier, *J. Phys. Chem. Solids*, 1998, **59**, 1241–1249.